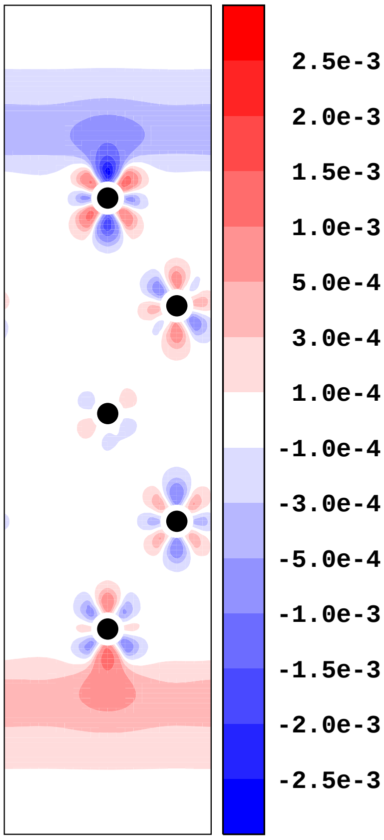

Figure 3.48: The change in the electron density of a Ru (0001) slab upon the application of a vertical electric field of 0.4 eV/Å

for some of the systems we show the density difference in the Figure 3.52. The calculations for Na/Rh (111) were performed with two substrate layers only because we only wanted to obtain a qualitative picture of the adsorption quickly. The density difference for K/Pt (111) looks very similar to the case of Cs/Ru (0001), but sodium on either platinium or rhodium – not shown – appears as qualitatively different; this is mainly due to the semi-core states of cesium and potassium, which are included as active states in these pseudo potentials, whereas in sodium the semi-core states were incorporated to the core and can thus not polarise at the surface. This choice of semi-core and valence is justified with the energetically deeper position of $2s$ and $2p$ states in sodium than of the corresponding states in potassium or cesium. Thus we believe this to be a real effect, and be due to the different chemical character of the sodium.

3.3.2 Adsorption of carbon monoxide on Ru (0001)

The adsorption of carbon monoxide on surfaces of transition metals has been studied by many experimental methods and semi-empirical and electronic structure methods – please see *e. g.* Over (1998) and references therein. On some of the transition metals – those on the left hand side of the periodic table – CO adsorbs dissociatively whereas on the surfaces of transition metals at the middle of the periodic table CO adsorbs molecularly. The adsorption on ruthenium and rhodium for example is molecular, with the molecular axis parallel to the surface normal (Dowben, 1997). Earlier, before the appearance of even qualitative studies using the low energy electron diffraction, the adsorption site was concluded mainly from the internal vibration C–O, a vibration at 1950 – 2100 cm^{-1} assigned to a one-fold on-top position, 1800 – 1950 cm^{-1} to two-fold bridge site and

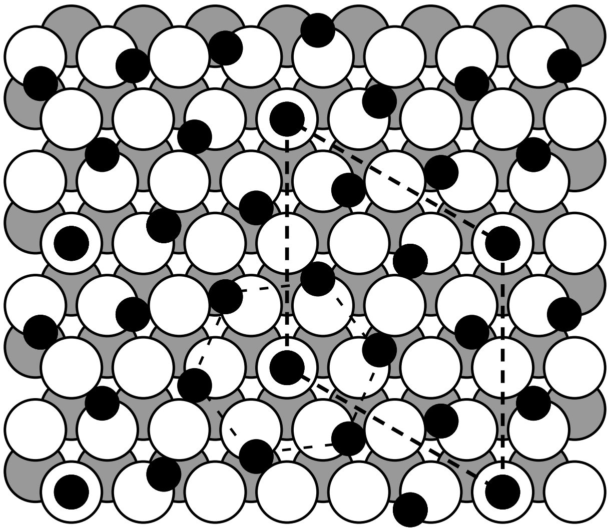

Figure 3.53: A suggested model for the $(2\sqrt{3} \times 2\sqrt{3})$R30° by Thomas and Weinberg (1979); the coverage is 7/12. Please notice the quasi-hexagonal, incommensurate arrangement of the molecules shown around one molecule

$(\sqrt{3} \times \sqrt{3})$R30° structure; this indicates an attractive second-nearest neighbour interaction, and since higher-concentration islands are not observed at any coverage, the nearest-neighbour interaction is either negligible or repulsive. The geometry of the high-coverage structure has not been qualitatively obtained but $(2\sqrt{3}\times2\sqrt{3})$R30° and $(5\sqrt{3}\times5\sqrt{3})$R30° structures are observed along coverages exceeding 1/3 by Thomas and Weinberg (1979), Williams and Weinberg (1979) and Braun *etal* (1997). The established interpretation is that compressed structures are formed when the coverage exceeds the 1/3; a suggestion by Thomas and Weinberg (1979) for the structure $(2\sqrt{3} \times 2\sqrt{3})$R30° is shown in the Figure 3.53. The compressed structures demands some of the CO molecules to adsorb also on sites other than the on-top site; this is possible if the adsorbate-adsorbate interaction dominates over the adsorbate-substrate interaction. Frequencies different from the ones found at the on-top site are expected but the change in the ν(C-O) is small between coverages 1/3 and the maximum coverage – please see below. The $(2\sqrt{3} \times 2\sqrt{3})$R30° structure is not observed in the low energy energy diffraction at room temperature (Pfnür *etal*, 1980); thus the corrugation of the adsorbate-substrate potential energy surface is very weak.

The Figure 3.54 shows the different eigenmodes of a two-dimensional molecule adsorbed along the surface normal. From these the frustrated translational and hindered rotational modes are parallel to the surface and thus do not create a dynamic dipole moment perpendicular to the surface; thereby the scattering amplitude of electrons *e.g.* in the high resolution energy energy loss spectroscopy is very small and the intensity negligible in the measurements. These modes can however be accessed *e.g.* with helium atom scattering (Braun *etal*, 1997) or methods accessing the diffraction of electrons (Over *etal*, 1993; 1995d; Gierer *etal*, 1996). The main observable in the vibrational measurements is usually only the internal ν(C-O) mode, and its variation at different coverages. If CO is adsorbed at low temperature 80 K the resulting over-layer is not fully ordered as concluded from the different frequencies than when dosing CO at higher a temperature; upon annealing the system dosed at a low temperature becomes equivalent to the structure adsorbed at higher temperature. Beyond the shift in the infra-red adsorption spectra shown in the Figure 3.55 Pfnür *etal* observed also a splitting of frequencies into two peaks; this appears also at coverages

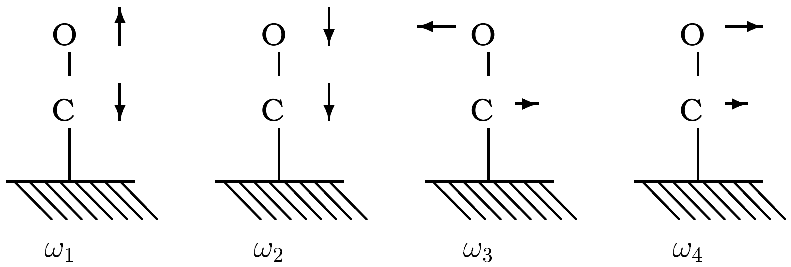

Figure 3.54: The vibrational modes of a dimer adsorbed in the up-right geometry on a surface

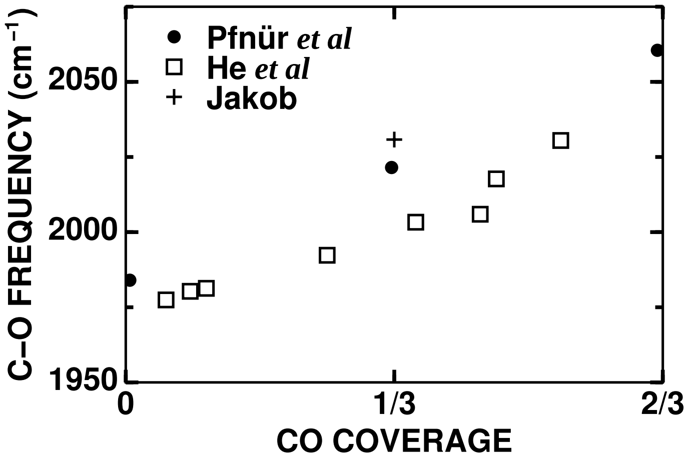

Figure 3.55: The vibrational frequency of CO from the infra-red adsorption spectroscopy by Pfnür *et al* (1980) and Jakob (1997) and the high-energy electron energy loss spectra of He, Dietrich and Jacobi (1996)

below 1/3 and is thus most likely due to molecules at island boundaries and their internals, or due to isolated molecules and molecules attached to islands.

Studies employing the scanning tunnelling microscope, at low temperatures due to the weak interaction and diffusion barrier, of the adsorption at low and high coverages might reveal the existence of island formation and the pattern of compressed structures, respectively, and are thus called for.

Geometry and energetics

We have performed density functional calculations for the CO adsorbed on Ru (0001) at different coverages from the (2×2) up to the mono-layer structure. The geometry of the principal structure $(\sqrt{3} \times \sqrt{3})$R30°-CO along with the model from the low energy electron diffraction measurements is shown in the Figure 3.56 and listed in the Table 3.12. The overall agreement is good, although the size of the vertical rumpling in the first layer is larger in the density functional calculations. The binding energy of CO in this structure is 1.83 eV; a desorption energy of 1.81 eV was obtained in the experiments of Pfnür, Feulner and Menzel (1983), showing an excellent agreement between the calculations and the experimental work; the energy difference between the on-top and the three-fold hollow hcp site was only about 60 meV, lower than what would be expected from the experiments where occupation of no other sites than the on-top sites has been observed even at high temperatures. Yet the low barrier for diffusion, 0.4 eV on the terrace at $\theta_{\rm CO} = 0.27$, fits to the result of a low corrugation of the potential energy surface for the adsorption of the CO. The change

Table 3.12: The geometry and electronic properties of CO adsorbed on the Ru (0001) in the $(\sqrt{3} \times \sqrt{3})R30^\circ$ structure as yield by our density-functional calculations and experiments by Michalk *et al* (1983) and Over, Moritz & Ertl (1993) – geometry –, and Pfnür, Feulner and Menzel (1983) – binding energy and change in the work function. The distance $z_{Ru_1-Ru_2}$ was calculated from the averaged layer positions

	DFT	Experiments
d_{C-O} (Å)	1.158	1.10±0.05
d_{Ru-C} (Å)	1.928	1.93±0.04
b (Å)	0.167	0.07±0.03
$z_{Ru_1-Ru_2}$ (Å)	2.102	2.08±0.04
$z_{Ru,bulk}$ (Å)	2.190	2.138
E_{bind} (eV)	1.83	1.81
$\Delta\phi$ (eV)	+0.79	+0.44

in the work function is largely over-estimated in our results, being almost two times too large. In the following we shall mostly analyse the adsorption of the CO in the (2×2) super-cell as we needed these results for the studies of the co-adsorption more than in the $(\sqrt{3} \times \sqrt{3})R30^\circ$ cell.

An interesting quantity is how the geometry and electronic properties are modified with a changing coverage; the Figure 3.57 collects these for CO/Ru (0001), and the Figure 3.55 contains the calculated frequency of the internal C-O stretching mode for CO/Ru (0001) and a hexagonal, free-standing mono-layer of CO. With the increasing coverage the C-O bond length decreases and the Ru-C distance increases, but the changes are very small; the change in the C-O bond length is much larger on the ruthenium surface than in the pure CO mono-layer. The change in the work function is qualitatively similar to the one in the experiments by Pfnür and Menzel (1983) but this time over-estimated by about 0.15 eV; the under-linear increase above the coverage 1/3 is reproduced in our calculations.

CO-CO interaction

In order to investigate the adsorbate-adsorbate interaction we performed the density functional calculations at different coverages; we did not go beyond the coverage 1/4 due to computational limitations. However, beyond the third- nearest neighbour interaction the CO-CO interaction is most likely small. We studied the structures (1×1)-1CO, (2×2)-3CO, $(\sqrt{3} \times \sqrt{3})R30^\circ$-2CO, (2×1)-1CO, $(\sqrt{3} \times \sqrt{3})R30^\circ$-1CO and (2×2)-1CO corresponding to the coverages 1, 3/4, 2/3, 1/2, 1/3 and 1/4. The interaction energies of the type of interactions shown in the Figure 3.58 were extracted like explained in the section in the Section 2.5.2; the molecule in the (2×2) structure was regarded as being isolated. The parameters thus obtained are given in the Table 3.13 with the same quantities fitted to desorption experiments by Payne, Zhang and Kreuzer (1992); it is seen that these two sets are rather similar to some extent but major differences occur. This does not surprise us considering that the numbers by Payne, Zhang and Kreuzer are derived semi-empirically and the neglect of the interactions beyond the third-nearest neighbour distance in the density functional study.

We shortly estimated the qualitative range of the CO-CO interaction from the dispersion of the 3σ and 4σ orbitals of CO, given in the Table 3.14: The major change occurs at the coverage 1/2 when the first nearest-neighbour sites become filled the dispersion increases rapidly, and a large

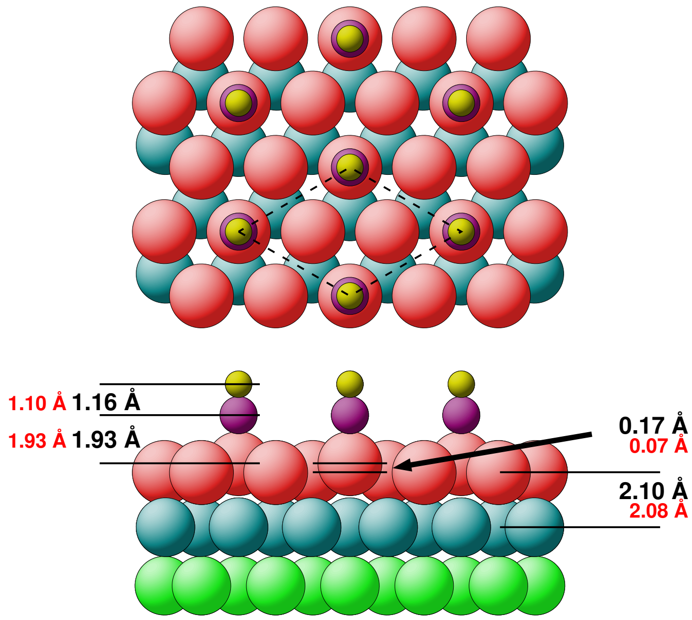

Figure 3.56: The geometry of CO in the $(\sqrt{3} \times \sqrt{3})R30^{\circ}$ structure from the density-functional calculations. The experimental values of Michalk *et al* (1983) and Over, Moritz and Ertl (1993) are indicated with the smaller font

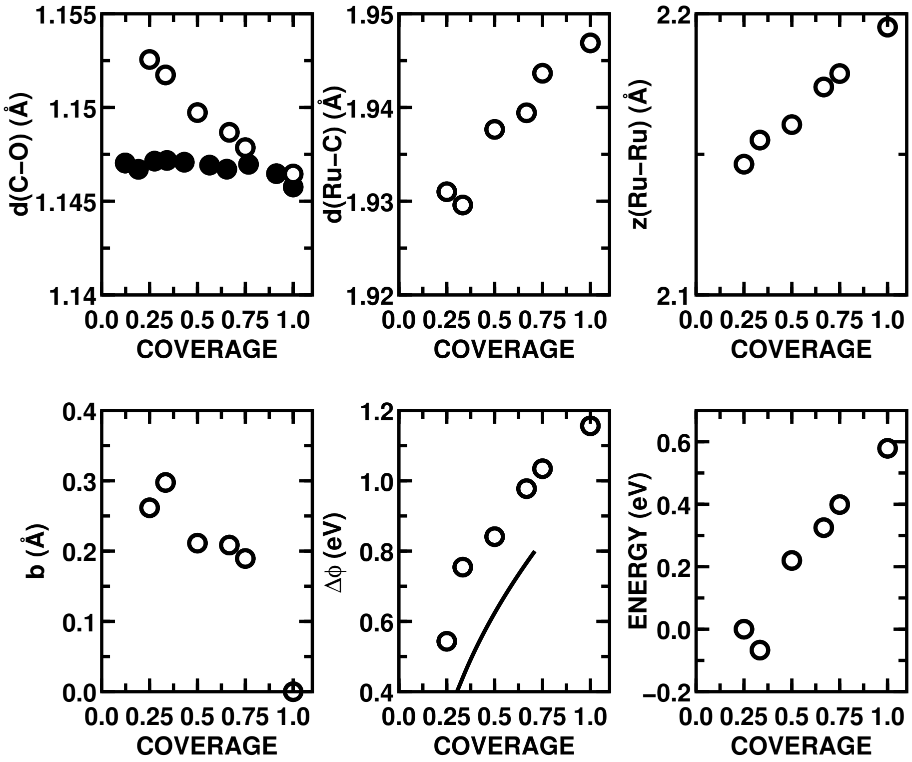

Figure 3.57: The geometry, binding energy and change of work function induced by the adsorption of the CO from the density-functional calculations; the binding energies are taken with respect to a molecule in the (2×2) structure, and b is the buckling in the first layer of the substrate. In the panel of the C-O distance the bond length of the CO in a hexagonal, free-standing mono-layer is included with filled circles, and in the panel of the change of the work function the experimental data from Pfnür and Menzel (1983) with a solid line

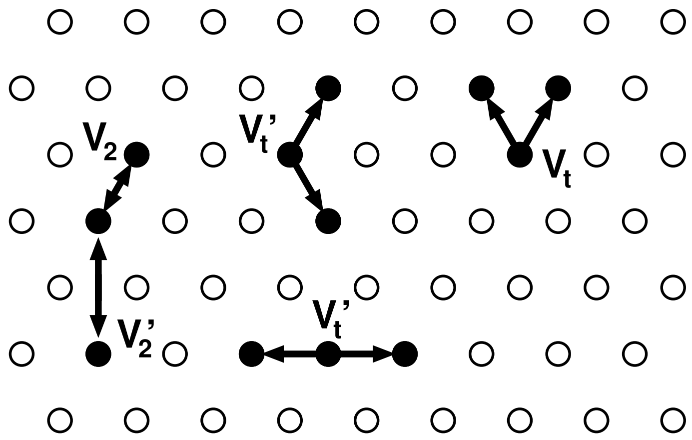

Figure 3.58: The definition of the parameters for the extraction of two- and three-particle interactions; all the CO molecules are placed at the on-top sites. V_t' and V_t" of the Figure 2.14 are set to equal as we do not have enough structures to differentiate them

Table 3.13: The two- and three-particle interaction parameters extracted from our density functional calculations; the fit to the experimental data is from Payne, Zhang and Kreuzer (1992). All values are in electron volts

	E_0	V_2	V_2'	V_t	V_t'
DFT	−1.76	0.157	−0.022	−0.098	+0.085
Fit	−1.59	0.124	+0.087	0.087	

jump occurs only upon at the distance of a (1×1) structure in the eigenvalues of a free-standing, hexagonal mono-layer of CO with the same density of molecules. This shows that the nearest-neighbour distance of 2.70 Å is a border-line for a strong inter-molecular interaction of the 3σ and 4σ orbitals.

Electronic structure

Next we shall analyse the electronic structure and binding of CO onto the ruthenium surface. We begin by showing the change in the total density of states in the Figure 3.60; the reference structure of CO is also calculated in the same super cell and thus contains a small but negligible contribution

Table 3.14: The dispersion of the 3σ and 4σ levels of CO at different coverages adsorbed on the Ru(0001) surface and a free-standing, hexagonal mono-layer of CO, marked with the sub-script ML; the dispersions are calculated from the Kohn-Sham eigenvalues at the **k** points of the self-consistent calculations and provide an equivalent sampling of the surface Brillouin zone

Coverage	3σ	4σ	$3\sigma_{\mathrm{ML}}$	$4\sigma_{\mathrm{ML}}$
1/4	0.00	0.01	0.00	0.00
1/3	0.00	0.04	0.00	0.01
1/2	0.30	0.79	0.04	0.11
2/3	0.42	1.11	0.09	0.21
3/4	0.44	1.19	0.19	0.29
1/1	0.64	1.71	0.59	1.00

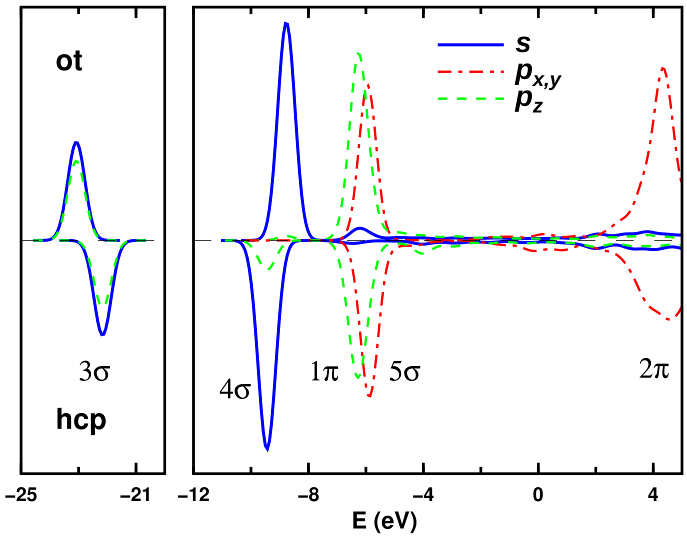

Figure 3.59: The density of states in the (2×2)-CO structure projected onto the s and p orbitals of the carbon atom; the corresponding plot for oxygen is very similar

from CO-CO interaction. The density of states projected on the atomic orbitals of the carbon in the Figure 3.59 provide a better insight to the character of the states contributing to the density of states at different energies. The position of the levels 3σ, 4σ, 1π and 5σ of CO are clearly identifiable: The σ orbitals only have s and p_z components whereas the π orbitals consist only of $p_{x,y}$ character. It is remarkable that the σ orbital at -6.2 eV lies below the π orbital; thus a theory based strictly on the frontier orbitals, in a molecular case the highest occupied molecular orbital – *HOMO* – and the lowest un-occupied molecular orbital – *LUMO* –, would face difficulties because the energetic ordering of the highest occupied orbitals has changed upon the adsorption.

The change in electronic density when the CO adsorbs on the Ru (0001) surface is illustrated in the Figure 3.62. The adsorption to the on-top and hcp sites leads into a similar change, and qualitatively the change agrees well with the Blyholder model: An increase is observed at the sides of the CO and a decrease along the axis of the molecule, just where the $2\pi^*$ and 5σ states are located, respectively. In the Figure 3.61 we also show some of the Kohn-Sham states which have a considerable magnitude at the CO molecule. The emerging picture resembles closely to that found by Hu *et al* (1995) for CO adsorption on Pd (110): the orbitals of the CO hybridise with the substrate states suggesting a chemical bond mechanism rather than a clear charge transfer from or to the highest occupied and unoccupied states as assumed in the Blyholder model. To clarify the hybridisation mechanism over the one suggested by the Blyholder model we show the projected densities of states in the Figures 3.64 and 3.65; in the former projected onto the σ and in the latter π Kohn-Sham orbitals of a CO molecule in the corresponding super-cell as the calculations of the adsorbed structure. The peaks are now clearly resolved according into the σ and π orbitals, and whereas the 1π and $2\pi^*$ mix only marginally, especially on the on-top site, the peak assigned to the 4σ contains some character of 5σ and vice versa. At the hcp site the difference is larger, 33 %, as also indicated in the Table 3.15 where the numbers were obtained by integrating the projected densities of states up to the Fermi energy. This effect is not in agreement with the Blyholder model, which states that the 4σ remains inert upon adsorption, but in qualitative agreement with the measurements of Nilsson *et al* (1997) who found a similar mixing of the 4σ and 5σ in the experiments. In the Section 3.4.2 we shall further discuss the consequence of the adsorption on

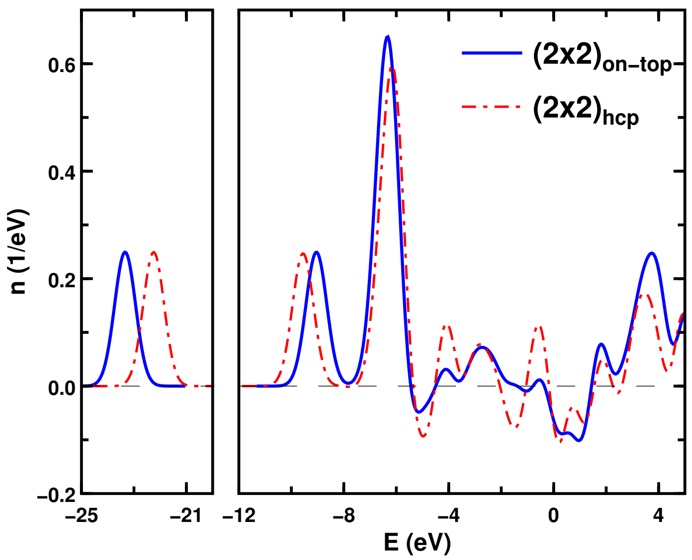

Figure 3.60: The change in density of states upon CO adsorption into the (2×2) structure on the on-top and hcp site

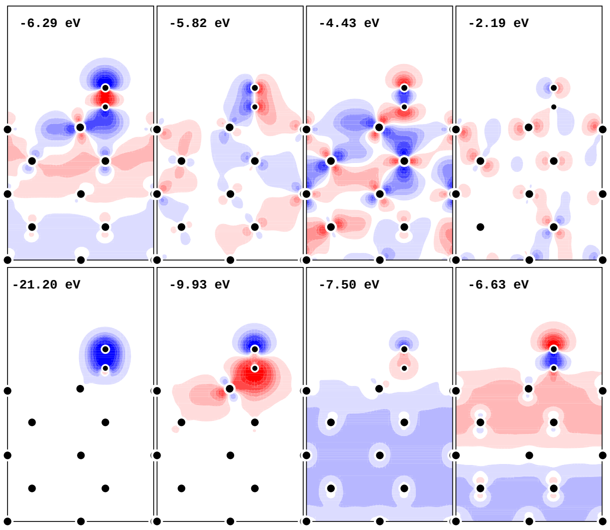

Figure 3.61: Some Kohn-Sham states at the Γ point of the Brillouin zone which have a considerable magnitude at the CO molecule in the (2×2)-CO_{hcp} structure

the different sites to the amount of the mixing.

Adsorption of N_2 versus CO

The adsorption of N_2 is often placed on a level with the adsorption of the iso-electronic CO, but sometimes a different mechanism is proposed; for a discussion of the issue please see de Paola *et al* (1987). Whereas the adsorption sites of the molecules are identical and the quantitative geometry very similar (Bludau *et al*, 1994) in the $(\sqrt{3} \times \sqrt{3})R30°$ structure, notable differences are *e.g.* the following:

- The work function increases upon the adsorption of CO but decreases when N_2 is adsorbed
- The internal stretching frequency C-O increases as a function of the coverage while the N_2 stretching frequency remains constant

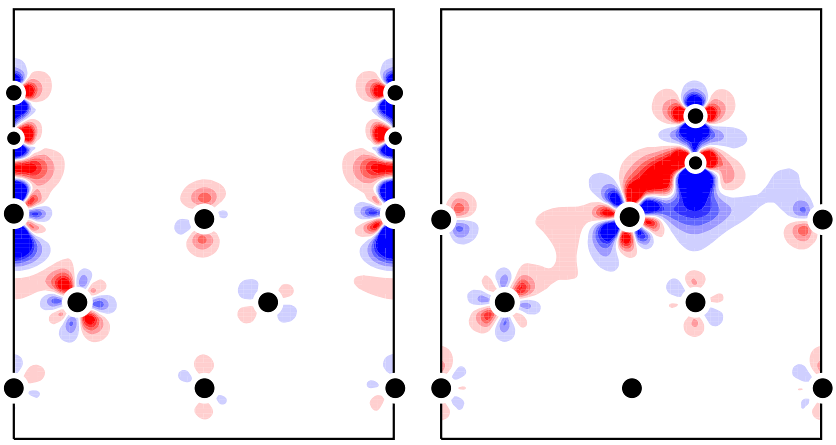

Figure 3.62: The change in the electron density upon CO adsorption into the (2×2) structure at the on-top – left – and hcp site – right

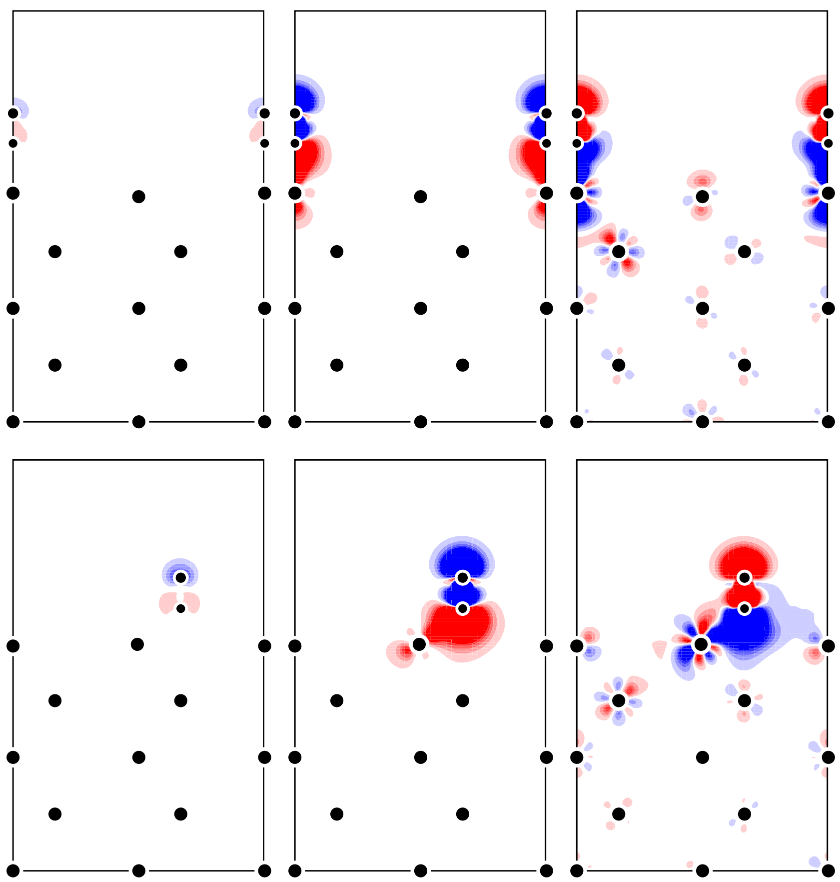

Figure 3.63: The change in electron density of the 3σ – left – and 4σ – middle – states and the rest of the valence electron density – right – upon CO adsorption into the (2×2)-CO structure at the on-top – top panels – and hcp sites – bottom panels

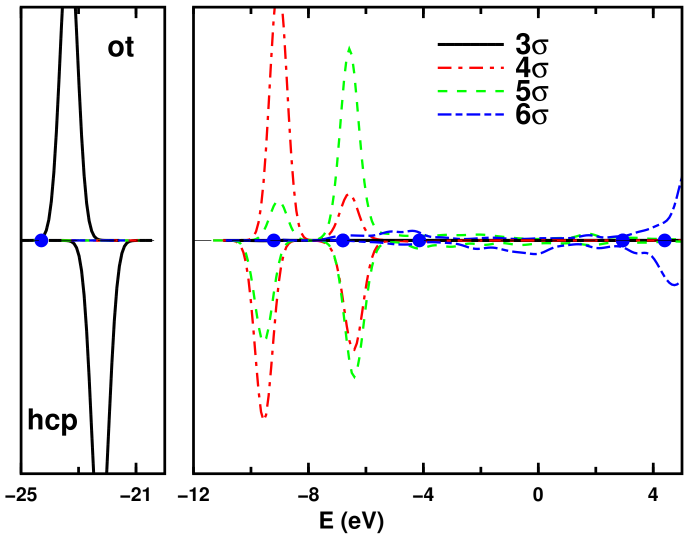

Figure 3.64: The density of states in the (2×2)-CO structure projected onto the molecular σ orbitals of the carbon monoxide. The dots indicate the Kohn-Sham eigenvalues of an isolated molecule; however the absolute location of them on the energy scale is arbitrary

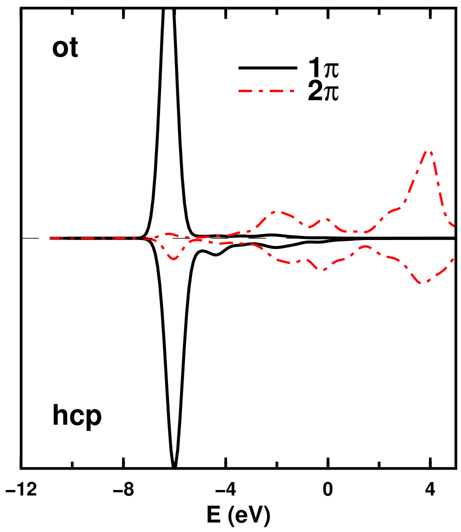

Figure 3.65: The density of states in the (2×2)-CO structure projected onto the molecular π orbitals of the carbon monoxide

Table 3.15: The occupation factors of different levels deduced from the projection of the Kohn-Sham states of the adsorption system on the molecular orbitals, and the mixing of 4σ and 5σ defined as the amount of molecular 5σ character of the 4σ in the adsorption system and vise versa. The results of Mortensen *et al* (1997) are included for Ru (0001)-($\sqrt{3} \times \sqrt{3}$)R30°-CO_{ot} and Ru (0001)-($\sqrt{3} \times \sqrt{3}$)R30°-$N_{2,ot}$

	Orbital						$4\sigma/5\sigma$
Structure	3σ	4σ	5σ	6σ	1π	$2\pi^*$	mixing (%)
Ru (0001)-($\sqrt{3} \times \sqrt{3}$)R30°-$N_{2,ot}$	1.000	0.992	0.974	0.226	0.998	0.159	16
Mortensen *et al*		0.990	0.970		0.997	0.175	
Ru (0001)-(2×2)-CO_{ot}	1.000	0.998	0.922	0.134	0.998	0.291	17
Mortensen *et al*		0.997	0.916		0.996	0.298	
Ru (0001)-(2×2)-CO_{hcp}	1.000	1.000	0.926	0.155	0.990	0.397	33

- The pre-adsorption of potassium prevents the co-adsorption of N_2, already at coverages of $\theta_K = 0.08$, whereas the adsorption of CO occurs up to high alkali coverages, and the alkali-CO interaction is attractive

The established explanation for these effects is along the lines of the Blyholder model, so that the 5σ orbital acts as a electron donator like in the carbon monoxide but the $2\pi^*$ orbital becomes much less occupied in N_2 than in CO. This model explain *e.g.* the lowering of the work function because the nitrogen dimer would lose part of its electrons and thus creates a dipole lowering the work function, and the repulsion with a co-adsorbed alkali atom is due to an electro-static repulsion. Mortensen *et al* (1997) addressed the difference between the adsorption of N_2 and CO on Ru (0001) based on calculations employing the density functional theory. In their results they indeed found a smaller occupation of the $2\pi^*$ in the case of N_2.

We also studied the N_2 onto the Ru (0001) surface, but only in the ($\sqrt{3} \times \sqrt{3}$)R30°-$N_{2,ot}$ structure. The resulting geometry in the Figure 3.66 agrees well with the results of Mortensen *et al* (1997), but the buckling of the first substrate layer in both calculations is not found in the measurements by Bludau *et al* (1994). In the calculations the buckling is about as large as in the case of the CO, and there the experiments gave a buckling – yet only half of the computed one – so a slight buckling due to the experimental analysis for the geometry of the N_2 on Ru (0001) cannot be excluded. The work function increases by +0.21 eV from the clean surface, thus in disagreements with the experiments (de Paola *et al*, 1987) which yielded a decrease of the work function by −0.52 eV. We obtained a value of 0.55 eV for the binding energy of the molecule to the surface in the ($\sqrt{3} \times \sqrt{3}$)R30°-$N_{2,ot}$ structure, close to the value obtained by Mortensen *et al* (1997), being much lower than the binding energy 1.83 eV of the CO agreeing well with the experimental trend. Mortensen *et al* explain this difference with the smaller overlap of the $2\pi^*$ state with the substrate states and thus a smaller energy gain from hybridisation; please compare the Figures 2.16 and 3.67, and note especially how both the 5σ and $2\pi^*$ have a larger weight on the carbon end in the CO than at the nitrogen ends of the N_2. The origin for the larger work function for the CO is apparent in the Figure 3.68, which shows the change upon the adsorption in the density averaged parallel to the surface: The density increases just above the outer-most substrate atom in the case of the nitrogen dimer, whereas the increase in the charge is close to the carbon atom for the carbon monoxide; this shift to further above from the surface increases the surface dipole and consequently the work function. It is

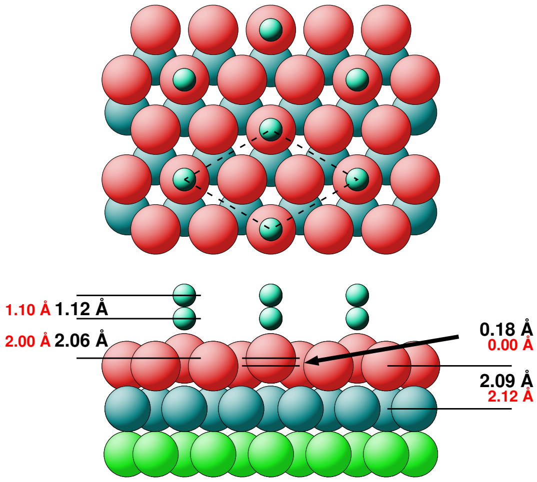

Figure 3.66: The geometry of N_2 in the $(\sqrt{3} \times \sqrt{3})$R30° structure from the density-functional calculations. The experimental values of Bludau *et al* (1994) are indicated with the smaller font

interesting that the difference in the adsorption energy of the N_2 between different adsorption sites is much larger than of the CO; the three-fold hollow sites are by 0.66 eV less favourable than the on-top site and thus only meta-stable against desorption. The largest difference in the electronic bonding mechanism between CO and N_2 is the deeper energy of the 4σ- and 1π-derived peaks, and the smaller occupation of the $2\pi^*$ orbital for the adsorbed N_2. The latter was also confirmed by the integral over the projected density of states in the Table 3.15.

We shortly studied the properties of the nitrogen dimer when the charge state and the relative population of the 5σ and $2\pi^*$ states was changed. Although the $2\pi^*$ state is anti-bonding a small filling increases the binding energy as seen from the Figure 3.69. The vibrational frequency decreases and the bond length increases monotonously when electrons are fractionally added to the molecule. The transfer of electrons from the 5σ to the $2\pi^*$ or the application of an electric field along the molecular axis affects the molecular properties similarly. These results also make implications to the effect of an added alkali metal to the adsorption and dissociation properties of the N_2 molecule; this was recently studied by Mortensen *et al* (1997; 1998; Mortensen, 1998).

The densities of states projected on the molecular σ and π states for the CO and N_2 adsorbed on the Ru (0001) are shown in the Figures 3.70 and 3.71, respectively. The σ orbitals of the two molecules are very similarly structured except for the lower location of the 4σ orbital of the N_2. The main peaks of the 1π and $2\pi^*$ orbitals in the nitrogen dimer are lower in energy but the $2\pi^*$ less occupied as was shown in the Table 3.15.

An interesting comparison to the experiments can be done between the Figure 3.72 and the results and conclusions by Nilsson *et al* (1997). The former shows the density of states projected onto the atomic orbitals of the nitrogen atoms in the structure Ru (0001)-$(\sqrt{3} \times \sqrt{3})$R30°-$N_{2,\mathrm{ot}}$, and in the latter the spatial distribution of the molecular orbitals were derived from the X-ray emission spectra. The arising picture from the calculations and these experiments along with the Blyholder model is shown in the Figure 3.73: The agreement between the calculational and experimental model is reasonable, considering that the experiments are for the Ni (100) surface and our calculations for the Ru (0001). However the agreement between the calculations and the experiments is superb, after the slight inaccuracy in the notation of the 4σ orbitals by Nilsson *et al* has been taken into account.

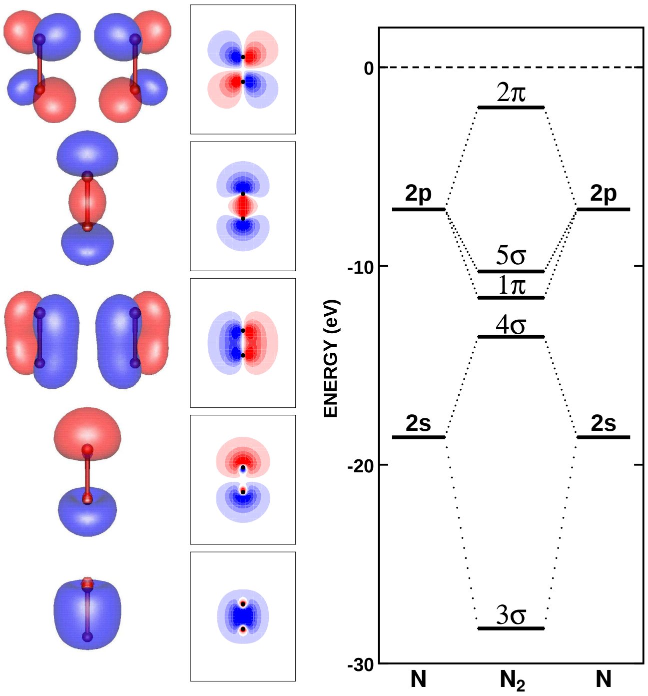

Figure 3.67: The significant Kohn-Sham single particle states of the nitrogen dimer; right are the energy levels of the orbitals from our density functional calculation. Please refer to the corresponding states of the carbon monoxide in the Figure 2.16

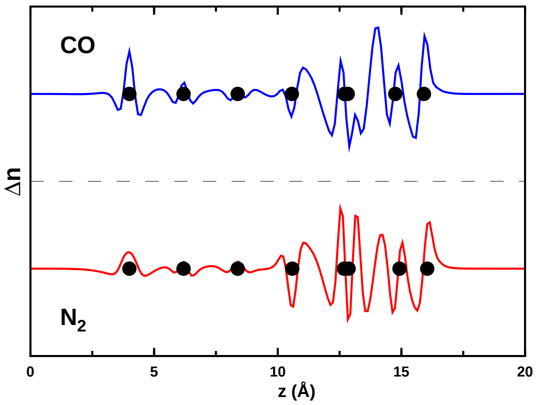

Figure 3.68: The change in electron density averaged parallel to the surface upon the adsorption of CO and N_2 to the Ru (0001) surface; the filled circles denote the atomic positions, and the dimers are the two right-most circles

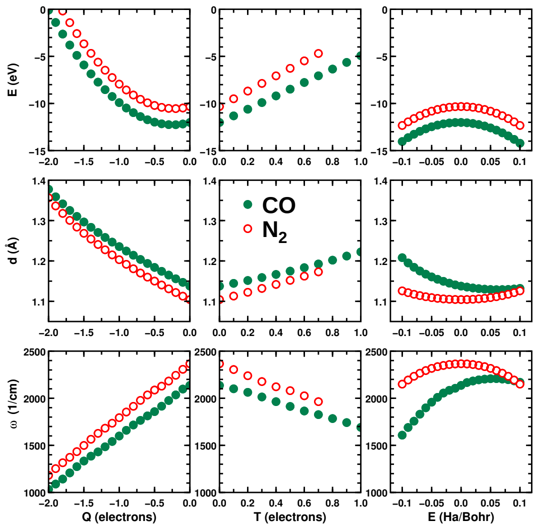

Figure 3.69: The binding energy – top panel, in electron volts –, bond length – middle panel, in Ångstroms – and vibrational frequency – bottom panel, in inverse centi-meters – of a carbon monoxide and nitrogen dimer as a function of the charge of the molecule Q – left –, the amount of the electron transfer $5\sigma \rightarrow 2\pi^*$ T – middle – and the magnitude of an electron field E along the molecular axis – right; the results were calculated with an all-electron cluster program. The green, filled circles denote results for the carbon monoxide and the red, hollow circles for the nitrogen dimer

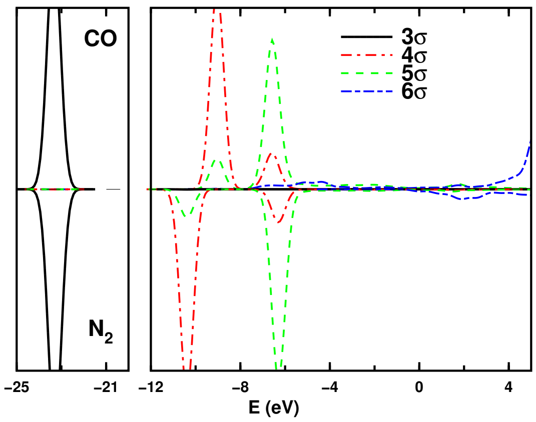

Figure 3.70: The density of states weighted with the projection of the molecular CO and N_2 σ orbitals to the Kohn-Sham states of the adsorption systems Ru (0001)-(2 × 2)-CO_{ot} and Ru (0001)-($\sqrt{3} \times \sqrt{3}$)R30°-$N_{2,ot}$

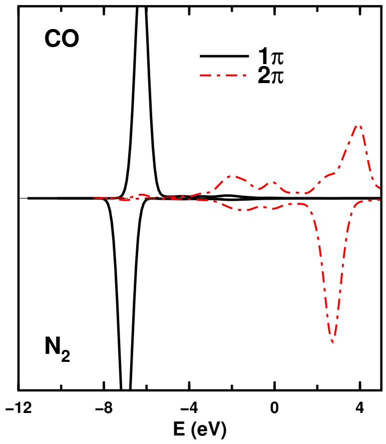

Figure 3.71: The density of states weighted with the projection of the molecular CO and N_2 π orbitals to the Kohn-Sham states of the adsorption systems Ru (0001)-(2×2)-CO_{ot} and Ru (0001)-($\sqrt{3} \times \sqrt{3}$)R30°-$N_{2,ot}$

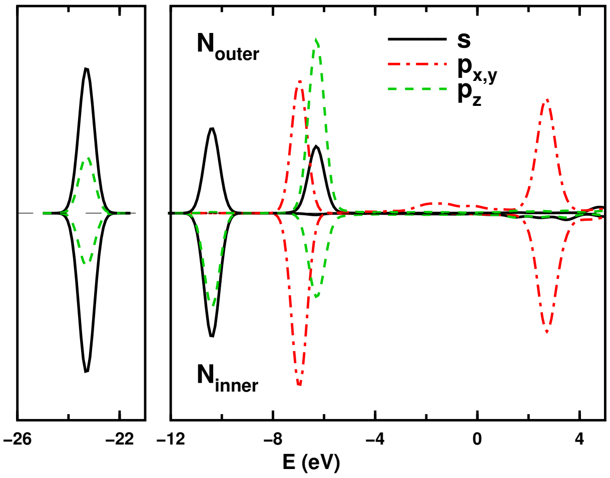

Figure 3.72: The density of states projected onto the atomic orbitals of the inner – *i. e.* closer to the surface – an outer nitrogen atoms in the structure Ru (0001)-($\sqrt{3} \times \sqrt{3}$)R30°-$N_{2,ot}$

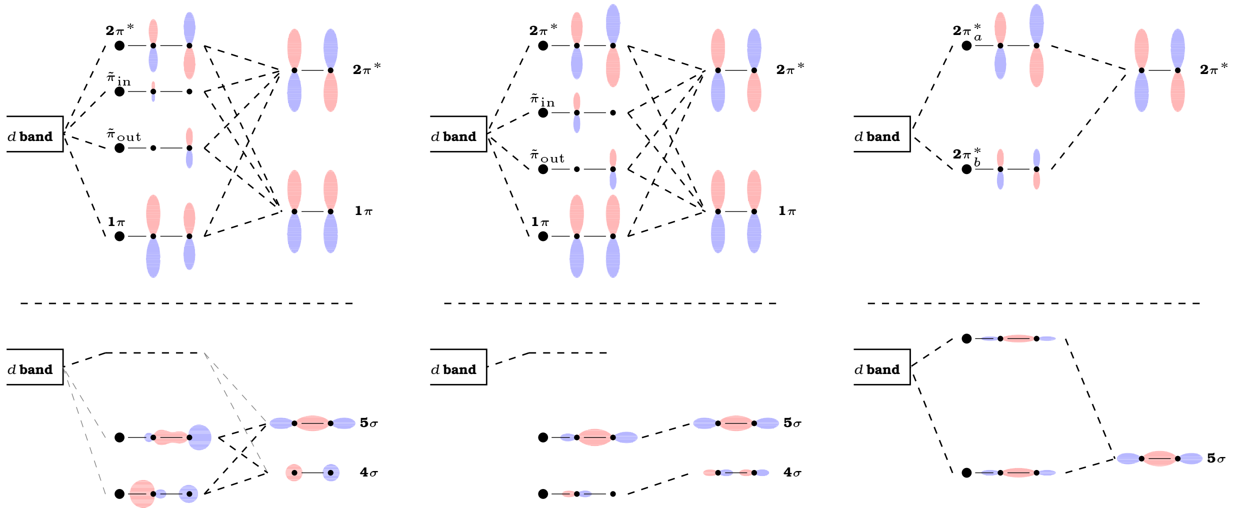

Figure 3.73: The schematic illustration of the molecular orbitals of the nitrogen dimer with the *d* bands of the substrate from our calculation – left –, the experiments of Nilsson *et al* (1997) – middle – and the Blyholder model – right; please notice that there is some inaccuracy in the notation of the 4σ orbitals by Nilsson *et al*

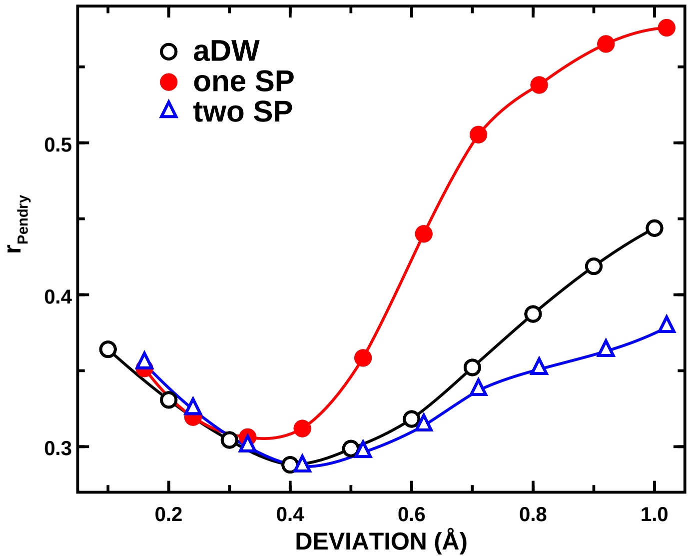

Figure 3.74: The r_P reliability factor for the temperature induced dynamic displacement of the oxygen atom defined as the root mean square deviation from the equilibrium position in the $(\sqrt{3} \times \sqrt{3})$R30°-CO structure at 150 K; from the low energy electron diffraction measurements of Gierer *et al* (1996). The different curves correspond to analysis with an an-isotropic Debye-Weller factor – aDW – and with one – one SP – and two – two SP – split-positions along the direction of the displacement

Vibrations of the CO

The CO molecule, since adsorbed parallel to the surface normal and bound to a single atom, and the heavier oxygen is the outer-more atom, the molecule can easily vibrate in the frustrated translational mode shown in the Figure 3.54. The recent measurement by Over *et al* (1995d; Gierer *et al*, 1996), using the concept of split positions (Over *et al*, 1993), were the first to investigate an anisotropic dynamical effect using low-energy electron diffraction. They obtained the r_P factor as a function of the displacement of the oxygen and carbon atoms – or, equivalently the tilt of the molecule – and were thus able to conclude the preferred displacement from the surface normal. The Figure 3.74 shows r_P as a function of the displacement of carbon and oxygen. From the minimum the tilt angle can be derived, and this is shown in the Figure 3.75 together with the results of Landskron *et al* (1996). The agreement in the two different experimental determinations – although both derived using the method of low energy electron diffraction – casts reliability on the result. A value for the frequency of the frustrated translational mode was further achieved by Over *et al*, being 5.5 ± 1.0 meV; it agrees well with the more established method to measure frequencies, the helium atom scattering, which provided a value (Braun *et al*, 1997) of 5.75 meV. Thus also the different methods yield frequencies very close to each other.

We studied the dynamic, temperature induced tilt with static calculations in the $(\sqrt{3} \times \sqrt{3})$R30° structure by determining the part of the potential energy surface which is necessary to investigate the dynamic movement of CO. These calculations were performed earlier than the other calculations in this works, with a different computer code and somewhat different calculational parameters due to computational restrictions. The `fhi94md` computer code – please see Stumpf and Scheffler (1994) or Kley (1997) – was used to perform the calculations, the plane wave cut-off was 40 Ry and a **k** point set with only one **k** point in the irreducible wedge of the surface Brillouin zone in the highly

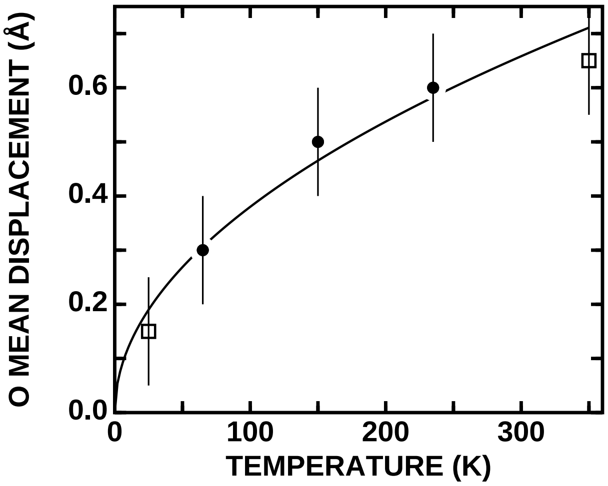

Figure 3.75: The dynamic displacement of the oxygen atom in the $(\sqrt{3} \times \sqrt{3})R30°$-CO structure from the low energy electron diffraction measurements of Gierer *et al* (1996) – filled circles – and Landskron *et al* (1996) – open squares

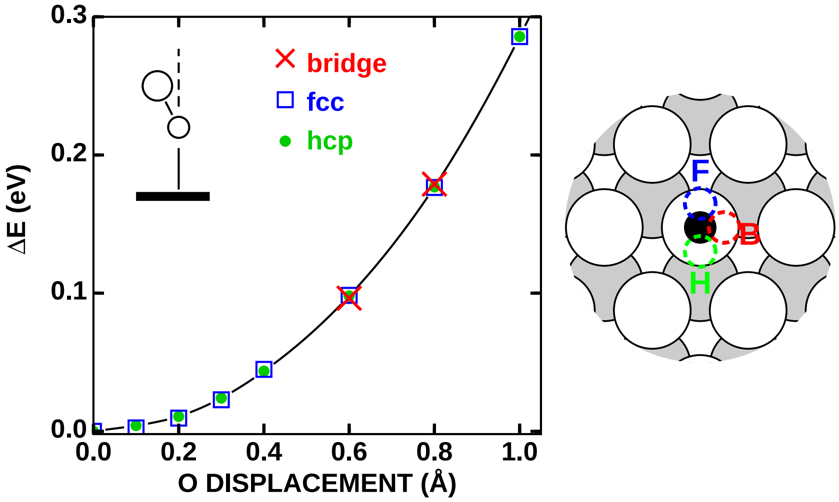

Figure 3.76: The change in energy upon a displacement towards different lateral directions of the oxygen atom from the equilibrium position in the $(\sqrt{3} \times \sqrt{3})R30°$-CO structure

symmetric case – in one twelfth of the full Brillouin zone.

First we studied the corrugation of the potential energy surface by moving the oxygen atom laterally away from the equilibrium site towards the different high-coordinated sites; due to the high symmetry the three directions – shown in the Figure 3.76 – this scans the whole azimuthal angle of 360° accurately enough. The carbon atom is kept fixed to save computational time; however, it would naturally be more affected by a lateral displacement due to its location closer to the surface. The change in energy as a function of the displacement of oxygen is given in the Figure 3.76. The corrugation seen by the oxygen atom is negligible and thus we conclude that the CO molecule can tilt with an equal probability into each direction; this is also supported by the electron stimulated desorption ion angular distribution measurements by Madey (1979). Thus in the subsequent calculations we considered only the tilt towards the hcp and fcc sites because in this case a mirror plane symmetry is conserved and less **k** points needed than for an arbitrary direction of the tilt.

We examined the energetics of the tilt both disallowing and allowing the relaxation of the carbon atom. The relaxation was performed by letting the carbon atom to move for each displacement of

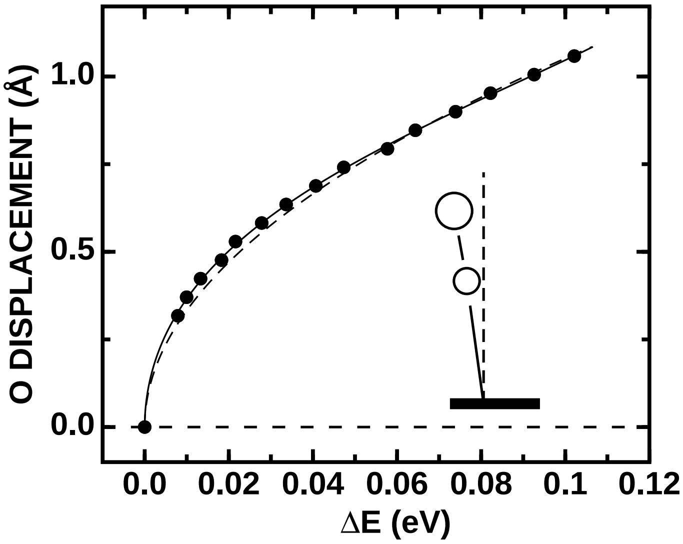

Figure 3.77: The lateral displacement of the oxygen atom from the equilibrium position in the $(\sqrt{3} \times \sqrt{3})$R30°-CO structure as a function of the change in the energy required; the carbon atom and the vertical coordinate of the oxygen are allowed to relax. The dashed and solid line correspond to a harmonic and anharmonic fit to the calculated points

the oxygen atom until the forces on the carbon atom and the vertical coordinate of the oxygen atom were zero. The energy versus displacement is shown in the Figure 3.77; near the minimum the curve resembles closely a harmonic potential and thus we shall in the following model the potential energy with the harmonic form

$$V(\Delta R) = \frac{1}{2} c\,(\Delta R)^2 \ . \tag{3.4}$$

The harmonic form has also the advantage that the displacements in the two directions x and y can be decoupled which is not the case in an anharmonic potential. ΔR is the lateral displacement of the oxygen atom, and the potential is assumed to be independent of the azimuthal angle due to small corrugation discussed above. Please note that we consider a static lateral displacement of the oxygen atom where all the other degrees of freedom are allowed to relax; to find the correct one the eigenmodes of the dynamical matrix should be calculated, but when the displacement is small the error is negligible. We shall consider only the case where the displacement of the carbon atom is allowed and thereby the mass of the vibrating particle is the mass of CO molecule. A fit to the calculated values gives a coefficient $c = 181$ meV/Å^2.

Since the molecule has two degrees of freedom it has a thermal energy of k_BT, or $\frac{1}{2}k_B$T per direction. The classical and quantum mechanical mean probabilities of displacement of a particle in a harmonic potential are

$$\overline{\Delta R_{\text{cl}}} = \sqrt{\frac{E_{\text{kin}}}{\mu\omega^2}} \tag{3.5}$$

and

$$\overline{\Delta R_{\text{qm}}} = \sqrt{\sum_{n=0}^{\infty} f_n \left(n + \frac{1}{2}\right) \frac{1}{\mu\omega}} \ , \tag{3.6}$$

respectively; μ is the mass of the oscillator and ω the frequency, and f_n the occupation of the mode n which depend on the kinetic energy and obey boson statistics. These classical and quantum mechanical results are shown in the Figure 3.78 together with the experimental ones.

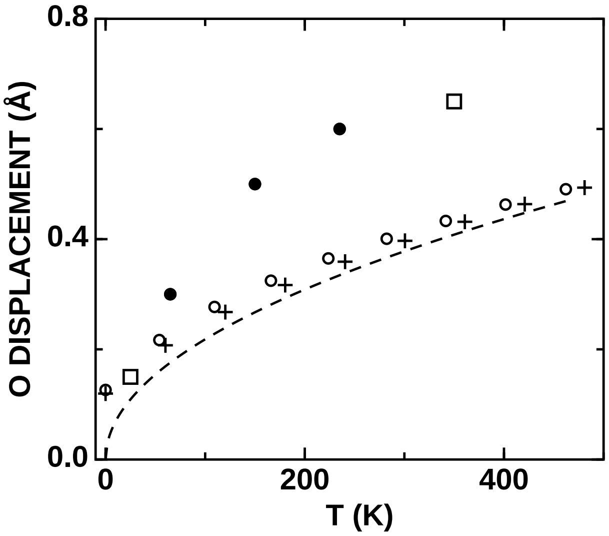

Figure 3.78: The lateral displacement of the oxygen atom from the equilibrium position in the $(\sqrt{3} \times \sqrt{3})$R30°-CO structure as a function of the temperature; the crosses are from a quantum mechanical calculation with a harmonic potential, the empty circles are from a quantum mechanical calculation with an anharmonic potential, the dashed line from a classical calculation with an harmonic potential and the filled circles and empty boxes are the experimental results

We further studied the effect of anharmonicity by fitting an anharmonic function to our potential energy shown in the Figure 3.77. Due to the isotropy only the even powers of the displacement occur in the fit and we use the function

$$V(\Delta R) = \frac{1}{2!}c_2\,(\Delta R)^2 + \frac{1}{4!}c_4\,(\Delta R)^4 + \frac{1}{6!}c_6\,(\Delta R)^6 \ . \tag{3.7}$$

The fitted coefficient are $c_2 = 0.137$ eV/Å^2, $c_4 = 1.149$ eV/Å^4 and $c_6 = -17.912$ eV/Å^6. We then solved the quantum mechanical probability function using a numerical program to solve the eigenstates of a particle in this potential. Please notice that there is an inherent error in our analysis because the two-dimensional potential energy surface is no longer exactly separable into two one-dimensional components; we expect the error to be small. The resulting displacement is shown in the Figure 3.78, and the results of the harmonic oscillator and experiments are shown for comparison; The agreement is seen to improve along the inclusion of the anharmonicity.

The frequency corresponding to the anharmonic fit is obtained either from the coefficient c_2 and is 4.31 meV or from the excitation energy from the lowest to the first excited state, yielding 4.65 meV. This is in a reasonable agreement with the experimental values 5.75 meV from the helium atom scattering by Braun *et al* (1997) and 5.5 meV from the low energy electron diffraction by Over *et al* (1995d; Gierer *et al*, 1996). The good agreement in both the vibrational frequency of the frustrated translational mode and the thermally induced tilt is not surprising since it is just this vibration which mostly causes the tilt. Over *et al* also suggest a very small displacemental amplitude in the direction perpendicular to the surface and thus a large anisotropy in the vibrations; this is easily understandable from the large difference in the frequencies of CO parallel ≈6 meV and perpendicular ≈50 meV to the surface, illustrating a much larger force constant for varying the Ru–C distance than the polar angle. For a system where CO adsorbs on a hollow site the anisotropy is probably much smaller, already due to the reduced Ru–CO frequency and furthermore due to a higher lateral corrugation.

3.3.3 Adsorption of carbon monoxide on other trigonal surfaces

We shortly discuss the adsorption of carbon monoxide also on other trigonal fcc (111) and hcp (0001) surfaces. The Table 3.16 shows a collection of the experimentally determined adsorption site of CO in the $(\sqrt{3} \times \sqrt{3})$R30°-CO structure on various group VIII and noble metal surfaces; please note that in addition to the $(\sqrt{3} \times \sqrt{3})$R30°-CO structure CO forms also other ordered, more complicated structures like the c(2×4)-2CO on Pd (111) and Pt (111), (2×2)-3CO on Rh (111) *etc*. On these surfaces CO adsorbs on-top except on Ni (111) and Pd (111); it is remarkable that on platinium, which has the same number of valence electrons as nickel and palladium, the CO adsorbs however at the on-top site. On the other hand the surface stress has a larger influence on Pt (111), and reconstructions on this clean surface are known. Also a definite structural analysis for the Pt (111)-$(\sqrt{3} \times \sqrt{3})$R30°-CO structure does not exist up to date and it is possible that this arrangement cannot exist as a long-order structure.

We performed density functional calculations for CO adsorption on the surfaces listed in the Table 3.17. The adsorption site is correctly reproduced at Ru (0001), Rh (111), Pd (111) and Ir (111) but on Pt (111) the calculations predict adsorption on the fcc site although from measurements it has been assigned to the on-top site. The differences in adsorption energy at different adsorption site in the Table 3.18 reveal the preference for the fcc site to be small but of the order of the energy differences on the other surfaces where the adsorption site was correctly predicted. Of the several possible sources for this discrepancy we believe the most likely are:

- The applied generalised gradient approximation for the exchange-correlation functional; this is always possible, although less probable since all the other cases are correctly reproduced. A recent calculation (Frank Wagner, personal communication) employing the local density approximation yields also the fcc site
- The pseudo potential approximation; this is unlikely since at least the carbon and oxygen pseudo potentials have shown good transferability so far. A recent all-electron calculation (Frank Wagner, personal communication) again agrees with our calculation
- The non-relativistic treatment of the valence electrons; however, relativity is actually included in the relativistically created pseudo potentials since the core electrons used to generate the pseudo atom have been calculated relativistically and thus the valence electrons, though calculated using the non-relativistic Kohn-Sham equation, sense the relativistic core *etc*. Recently Pacchioni *et al* (1997) calculated the adsorption of CO on several group VIII metals and found the relativity, already when included at the scalar relativistic level, to reproduce the correct adsorption site but a non-relativistic calculation gave the same discrepancy as in our results

The adsorption energies along the rows of the periodic table decrease the more the *d* shell is filled. This is probably due to the more compact structure of the almost filled *d* bands, thus making extra bonding or hybridisation less likely.

Hammer, Morikawa and Nørskov (1996) also made a study of the CO adsorption on metal surfaces. However, they did not relax the system and placed the CO molecule always on the on-top site. They obtained a very good agreement between the fully self-consistent adsorption energies and values predicted from a tight-binding type of model as shown in the Figure 3.79; the quality of correspondence of the model and self-consistent calculation casts confidence to the applicability of the model. The point of intersection – ≈0.45 eV – gives the interaction energy of CO with

Table 3.16: The experimental adsorption site of CO on fcc (111) and hcp (0001) trigonal surfaces of group VIII and noble metals. The adsorption structure is always $(\sqrt{3} \times \sqrt{3})$R30°-CO. The data are extracted from Wei, Skelton and Kevan (1997) except Co (0001) which is measured by Lahtinen, Vaari & Kauraala (1998)

	Co ot	Ni fcc	Cu ot
Ru ot	Rh ot	Pd fcc	
	Ir ot	Pt ot	

Table 3.17: The adsorption site of CO determined by our density functional calculations on fcc (111) and hcp (0001) trigonal surfaces of group VIII and noble metals. The adsorption structure is always $(\sqrt{3} \times \sqrt{3})$R30°-CO

			Cu fcc
Ru ot	Rh ot	Pd fcc	
	Ir ot	Pt fcc	

Table 3.18: The adsorption energy of CO determined by density functional calculations on fcc (111) and hcp (0001) trigonal surfaces of group VIII and noble metals. The adsorption structure is $(\sqrt{3} \times \sqrt{3})$R30°-CO in all the cases. Negative values are the binding energies at the preferred adsorption site and the positive values differences to this value; all values are in electron volts. The emphasised values are experimental values listed by Hammer, Morikawa and Nørskov (1996) except Rh (111) which is from Wei, Skelton and Kevan (1997)

	on-top	fcc
Ru (0001)	−1.83	+0.22
	−1.66	
Rh (111)	−1.75	+0.04
	−1.79	
Pd (111)	+0.50	−1.87
		−1.47
Ir (111)	−1.99	+0.53
Pt (111)	+0.13	−1.62
	−1.50	

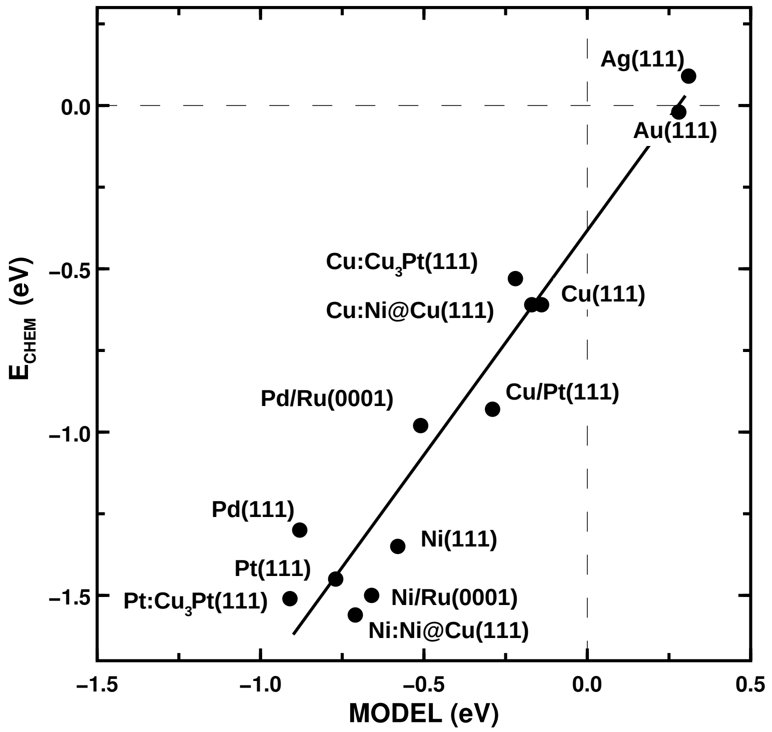

Figure 3.79: The adsorption energy of CO from the Newns-Anderson model versus the self-consistent density functional calculation in a model geometry in the $(\sqrt{3} \times \sqrt{3})R30°$-CO structure; from Hammer, Morikawa and Nørskov (1996)

the *s* and *p* electrons, in good agreement with the values for Al (111), whereas the change between different elements arises from the interaction of CO $2\pi^*$ and 5σ states with the transition metal *d* bands; Hammer, Morikawa and Nørskov conclude their results to be in good agreement with the prediction of the Blyholder (1964) model and the studies of Bagus and Pacchioni (1992). Hammer, Morikawa and Nørskov also discuss the correlation between the core level shifts of the transition metals and the CO chemisorption energy observed by Rodriguez and Goodman (1992) and later studied theoretically by Weinert and Watson (1995) and Hennig, Ganduglia-Pirovano and Scheffler (1997).

We finally show the changes of work function in the Table 3.19; the differences between different adsorption sites are large and although the magnitude of the changes is most likely overestimated the determination of the adsorption site based on the change in work function should still be possible. That the work function is higher at the three-fold site in all cases studied here is in line with the observation that the emptying of the 5σ orbital – located mostly at and below the carbon atom – and filling of the $2\pi^*$ – having more weight at both atoms – would shift the centre of average charge further away from the substrate, leading to an increase in the work function. Along the rows of the periodic table the change in work function decreases with the binding energy, and the change is less positive – even negative at Pt (111) – at the 5*d* metals than at the 4*d*'s.

3.3.4 Adsorption of oxygen

Since the adsorption of oxygen is not central for the present work we shall here only list the main properties relative to the similar adsorption system of nitrogen on Ru (0001), which was recently studied by Schwegmann *et al* (1997). The major differences between N/Ru (0001) and O/Ru (0001)